HiSST: 2nd International Conference on
High-Speed Vehicle Science & Technology

16–19 May 2022, Bruges, Belgium

Low fidelity design and analysis of propulsion systems for high-supersonic cruiser concepts

Bora O. Cakir [1,2], Ali Can Ispir [3], Bayindir H. Saracoglu [4]

Abstract

Ramjet/scramjet propulsion is commonly preferred to power supersonic & hypersonic vehicles for cruising faster than Mach 3. This is an elegant solution owing to the lean architecture which does not embody any rotating parts. Although the geometry of the engine is simple as compared to turbo-based engines, the flow physics through the engine duct is quite complex and, the flow speeds modulate between the supersonic and subsonic regimes. The design and performance analysis of such engine configurations are vital to make sure that propulsion systems can satisfy the flight trajectory requirements. In the present study, a low fidelity design and analysis methodology is introduced to investigate the propulsive performance characterizations of different design choices on intake configurations, providing complete propulsive flow path simulations via subsonic combustion, thermal choke phenomena and ideal expansion through the nozzle.

Keywords: *Reduced order modeling, Propulsive performance, High-speed intake design, Ramjet engine, Detailed chemistry*

Nomenclature

Latin

A – Area [m^2]
C_f – Skin friction coefficient
C_p – Specific heat [J.kg^{-1}.K^{-1}]
D – Hydraulic diameter [m]
ER – Equivalence Ratio
$\dot{m}$ – Mass flow rate [kg.s^{-1}]
M – Mach number or Reaction number
MW – Molecular weight [kg.mol^{-1}]
P – Pressure [Pa]
Pr – Prandtl number
Q – Progress rate
T – Temperature [K]
U – Velocity [m/s]
X – Molar concentration [mol.m^{-3}]
Y – Species Mass Fraction

Greek

ϵ – Flow direction parameter
γ – Specific heat ratio
ρ – Density [kg/m^3]
$\dot{\omega}$ – Molar production rate [mol.m^{-3}.s^{-1}]

Subscripts

0 – stagnation
C, I – combustor inlet
i – species index
I, E – inlet exit
w – wall

1. Introduction

Flight operation at high supersonic speeds relate to severe aerodynamic and structural demands which challenges the efficiency reliability and durability of the relevant design elements. Furthermore, the mis-

[1] *Doctoral Candidate, von Karman Institute for Fluid Dynamics (VKI), Turbomachinery and Propulsion Department, Chaussée de Waterloo 72, Rhode-Saint-Genese, bora.orcun.cakir@vki.ac.be*
[2] *Doctoral Student, Lund University, Department of Energy Sciences, Ole Römers väg 1 (5:e vån), Lund*
[3] *Doctoral Candidate, von Karman Institute for Fluid Dynamics (VKI), Aerospace and Aeronautics Department, Chaussée de Waterloo 72, Rhode-Saint-Genese*
[4] *Research Expert, von Karman Institute for Fluid Dynamics (VKI), Turbomachinery and Propulsion Department, Chaussée de Waterloo 72, Rhode-Saint-Genese*

sion definition of a high-speed cruiser also corresponds to wide range of operating conditions, including significant airspeed and altitude variations. Hence, the aircraft is required to perform relatively well in low-speed & low-altitude conditions for take-off and landing operations, accelerate over a wide spectrum of Mach numbers and finally be able to efficiently cruise at the designated speed and altitude [1]. Therefore, configuration, investigation and optimization of a high-speed propulsive system constitutes a crucial milestone for the design procedure of a supersonic/hypersonic aircraft as well as the practical realization of supersonic flight in civil aviation.

Accordingly, a wide range of airbreathing propulsion systems are developed for supersonic/hypersonic cruiser concepts. Depending on the design requirements, these systems comprised various levels of interaction with the airframe of the lifting body where the distinction between integrated and standalone propulsion plants arose. Comparing the empirically deriven maximum L/D relations valid for supersonic/hypersonic flight regimes with the hypersonic vehicles, it was concluded the shape of the vehicle should be contributing the overall aerodynamic performance by generating an extra compression process [2]. In this regard, the vehicle configuration should be equipped with a highly integrated propulsive plant that can provide enhanced aerodynamic efficiency while ensuring a net positive thrust [3]. Thus, many studies focusing on conceptual and practical design of high-speed aircraft employed integrated engine configurations with the main airframe [4, 5, 6].

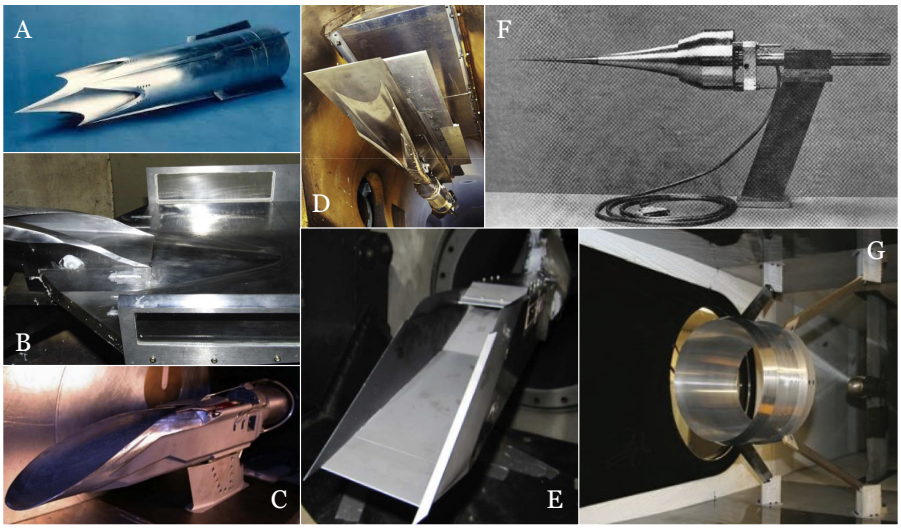

Fig 1. Experimental configurations of hypersonic wavecatcher intakes: (A) The JHU/APL four-module intake on a SCRAM model [7]. (B) Three-dimensional bump-integrated IWI [8]. (C) Streamtraced intake with circular capture streamtube [9]. (D) REST intake by NASA Langley Research Centre [10]. (E) HyShot II planar scramjet intake model [11]. (F) The Oswatitch hypersonic intake [12]. (G) Fully enclosed Busemann intake [13].

On the effort of designing high-speed air intakes for supersonic and hypersonic propulsion systems, a great emphasis is made on performing the compression on incoming air stream isentropically in order to minimize the losses. However, inevitable appearance of shock waves limits this capability in the sense that their presence has to be accommodated in the least destructive manner possible from an efficiency point of view. Various approaches are available to achieve that where regardless of the geometrical differences, the main similarity of compressing the freestream air through a series of weak compression waves and proceeding shock systems reveal a common point for design constraints. The different approaches dictating the geometrical contours, as a result topology of flow structures, can be distinguished as planar and axisymmetric shapes. Intake designs with a planary symmetric geometrical structure, also referred to as the Prandtl-Meyer intakes, contain the fluid flow by side walls while the compression is performed isentropically over a ramp by flow turning followed by an oblique shock wave [14]. As the sidewall interactions yield three dimensional flow structures disrupting the planar symmetry of the flow

topology, their influence on the compression process is identified via multiple high fidelity simulations and detailed experimental investigations [15, 16, 17]. Moreover, the preliminary contouring of the intake designs based on axisymmetric flow templates, can be divided in two main groups depending on the flowpath geometries; inward [18] or outward turning intakes [19]. Inward tuning intake geometries are of a converging nature where the incoming flow direction is gradually altered towards the central axis of the intake. As a result, weak compression waves reduces the flow speed and increases its static pressure isentropically by focusing the at a common coalescence point to prevent any premature shock wave generation [20, 18]. The design procedure for these type of intakes involve a low fidelity flow characterization generally based on method of characteristics [21] and streamtracing approach for extraction of the three-dimensional geometrical layouts [22].

Ramjet and scramjet engines are air-breathing propulsion systems which can provide seamless operation along supersonic and hypersonic flight regimes. One of the methods commonly used for analysis of high-speed propulsive flow paths is solving one-dimensional inviscid flow equations along the engine duct. This approach enables a cost-effective performance estimation for conceptual design studies compared to high-fidelity CFD simulations [23, 24]. Accordingly, Torrez et al. developed a one dimensional model to investigate the precombustion shock and dissociation effects in scramjet engine [25]. Birzer and Doolan modeled a hydrogen-fueled scramjet combustor by using a one-dimensional ODE set and validated their approach with Hyshot-II experimental cases [26]. Furthermore, while the flow regime is fully supersonic in scramjet engines, incoming flow is compressed and decelerated to subsonic conditions by the shock waves in the intake and isolator parts of the propulsion duct. The air flow is mixed with the fuel and burned under subsonic regime then the exhaust flow is anticipated to reach sonic condition in the combustor exit, known as thermal choking [27]. Therefore, many efforts were spent for design and analysis of the ramjet engines with respect to thermal choking phenomena [28, 29]. In this regard, Torrez et al. expanded and coupled Shapiro method with MASIV propulsion code to make prediction for thermal choking position i.e. mathematical singularity in the engine duct [30]. Villace et al. used mass flow parameter formulation to impose thermal choke to the exit of ramjet combustor, the mass flow rate of the fuel is computed to satisfy this condition [31].

Even though there exits a large variety of low-fidelity design and analysis studies for accurate characterization of combustion performance specifications, the upstream conditions for the combustion process is generally provided by means of user defined variables or the intake performance specifications computed using high fidelity simulations. Hence, there is no prior attempt to couple the intake design approaches with a combustion analysis module. Therefore, the proposed design tool combines the individual design and analysis approaches for high-speed propulsive path components to achieve a holistic low-fidelity design method for cost-efficient characterization of a high-speed propulsive design space. Accordingly, the introduced analysis methodology is employed to investigate the intake design considerations and their influences on the propulsive performance for ramjet engines as a case study.

2. Methodology

A ramjet/scramjet propulsive flow path is composed of an intake, an isolator, a combustor and a nozzle [32]. As the proposed design tools aims to achieve a coupled full flow path optimization, it comprises of four main modules. The intake design process and the related design constraints for the selected configuration is introduced in Sec. 2.1. The description of the isolator design considerations is given in Sec. 2.2. Then, the use of aforementioned considerations on the combustion analysis and their interaction with the other components for combustor design is discussed in Sec. 2.3. Finally, the nozzle design module is mentioned as the most downstream component of the propulsion system in Sec. 2.4.

2.1. Intake design module

The intake configuration is determined according to the design needs of a generic high-supersonic cruise vehicle with a highly integrated propulsive plant. Referring to the highly three dimensional flow formations over the aerodynamic contours of waveriders, and the performance specifications and structural integrity demands of combustors, an axisymmetric flow geometry described over a circular cross-section is required for the intake design [33]. Furthermore, in order to achieve the necessary flow compression through the intake while keeping the intake length within a practical range, all supersonic/hypersonic

intake designs include an isentropic compression proceeded or superceeded by an oblique shock wave [34, 35].

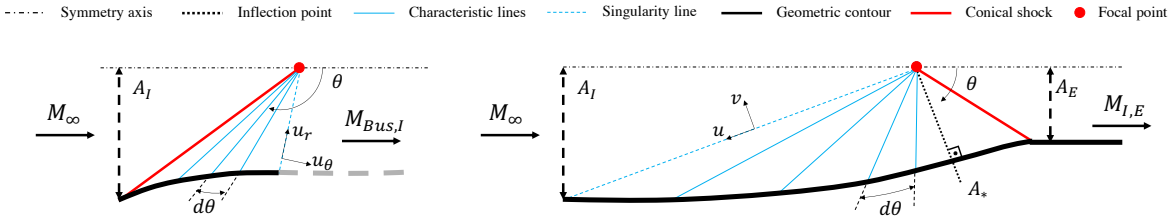

Fig 2. Schematics for the internal compression flows of ICFA (left) and Busemann (right) diffuser.

Concentrating on internal axisymmetric flows, three different types of conical flow patterns are introduced by Mölder [36]. Among these, the Busemann diffuser and Internal Conical Flow A (ICFA) were identified to reveal a convergent behavior, as the incoming flow is compressed and decelerated. The ICFA, schematically represented in Fig.2 (left), starts with an internal conical shock wave followed by an isentropic compression region downstream. The axsiymmetric contours enclosing the ICFA yield a singularity as the angular velocity approaches to sonic condition. On the other hand, the Busemann diffuser is defined as an isentropic compression field constructed by means of a series of compression waves followed by a trailing shock wave that terminates the compression process and realigns the flow with the central axis (Fig.2, right). Opposite to the ICFA, the singularity point of a Busemann diffuser occurs where the incoming airstream meets the leading edge.

The template for any axisymmetric, conical flow formation can be described by the streamtube shapes derived based on a two dimensional Taylor-Maccoll (T-M) flow
citeemanuel2001 and it is shown that the validity of the T-M flow can be extended to a three dimensional space [37]. The T-M flow 's are descirbed by two linearyed first order T-M equations [38] and can be recast by the radial, u, and angular, v Mach numbers [13].

$$\frac{du}{d\theta} = v + \frac{\gamma - 1}{2} uv \frac{u + vcot(\theta)}{v^2 - 1} \tag{1}$$

$$\frac{dv}{d\theta} = -u + (1 + \frac{\gamma - 1}{2} v^2) \frac{u + vcot(\theta)}{v^2 - 1} \tag{2}$$

with a corresponding streamline definition provided by Eq.(3).

$$dr/d\theta = ru/v \tag{3}$$

Moreover, the ICFA can also be described by the T-M equations since it also satisfies the conical symmetry. Thus, the flow characterization downstream of the leading edge conical shock is established by Eqs. (4),(5) and (6).

$$\frac{du_\theta}{d\theta} = \frac{(\gamma - 1)(2u_r + u_\theta cot(\theta))(1 - u_r^2 - u_\theta^2)}{2(u_\theta^2 - a^2)} \tag{4}$$

$$\frac{du_r}{d\theta} = u_\theta \tag{5}$$

$$a = \sqrt{(\gamma - 1)(1 - u_r^2 - u_\theta^2)} \tag{6}$$

where u_r and u_θ are the radial and angular velocities normalized with the escape speed, and a is again the local speed of sound computed by means of u_r and u_θ.

The T-M equations described above for the two axisymmetric flow templates of the ICFA and the Busemann diffuser are ordinary differential equations (ODE) that specify initial value problems (IVP). Therefore, proceeding to the definition of the proper initial conditions, the Eqs.1&2 and 4&5 can be solved with a numerical integration scheme of Runge-Kutta 4 (RK4)[39]. The main difference between the numerical descriptions of the solutions of ICFA and Busemann flows is the integration direction. The numerical integration of Eqs. (4), (5) and (6) is initiated with the flow properties just downstream of the conical oblique shock and proceeded in the downstream direction. On the contrary, Eqs. (1) and (2), are solved with an integration starting with flow properties just upstream of the trailing shock and proceeding towards the upstream direction. Therefore, the initial conditions for the both IVPs are determined by means of the oblique shock relations with the predefined freestream and intake exit conditions [37].

2.2. Isolator design module

The inlet configurations under investigation are distinguished via the strength of the terminating conical shockwave. In case of subsonic flow conditions at the exit of the Busemann diffuser, the terminating shock is referred to as a strong shock across which the supersonic flow is decelerated substantially to subsonic conditions. Contrarily, in case the exiting flow is still supersonic, the terminating shock is considered to be weak such that a high total pressure recovery is maintained. Therefore, as the case study of ramjet engines require subsonic flow conditions at the inlet of the combustion chamber, the weak shock configurations are coupled with a normal shock assumption to replace the isolator component [40].

2.3. Combustor design module

Flow through the combustor of the ramjet engine is modeled by quasi-one-dimensional equations of motion coupled with reaction terms resolved by detailed chemistry approach [41]. The reaction rates are calculated by a detailed chemistry mechanism including 33 reactions among 13 species [42] where the thermophysical properties of each species are computed with the data in supplied JANAF thermochemical tables [43]. The governing equations are constructed to handle subsonic & supersonic flows throughout the ramjet combustor and nozzle. The incoming air and fuel streams are assumed to be perfectly mixed downstream of the fuel struts which is located at the beginning of the combustor section.

$$\frac{1}{\rho}\frac{d\rho}{dx} = \frac{1}{\dot{m}}\frac{d\dot{m}}{dx} - \frac{1}{U}\frac{dU}{dx} - \frac{1}{A}\frac{dA}{dx} \tag{7}$$

$$\frac{1}{U}\frac{dU}{dx} = \frac{-1}{\gamma M^2}\left(\frac{1}{p}\frac{dp}{dx} + \frac{2\gamma M^2 C_f}{D} + \frac{\gamma M^2(1-\epsilon)}{\dot{m}}\frac{d\dot{m}}{dx}\right) \tag{8}$$

$$\frac{dT}{dx} = \frac{1}{C_p}\left(- \sum_i (h_i \frac{dY_i}{dx}) + [\frac{1}{\dot{m}}\sum_i \left(h_i (\frac{d\dot{m}_{i,added}}{dx}) \right) - \frac{h_0}{\dot{m}}\frac{dm}{dx}] - \frac{2C_f C_p (T_{aw} - T_w)}{Pr^{2/3} DA} - U\frac{dU}{dx} \right) \tag{9}$$

$$\frac{dY_i}{dx} = \frac{\dot{\omega}_i M W_i A}{\dot{m}} + \frac{1}{\dot{m}}\frac{d\dot{m}_{i,added}}{dx} - \frac{Y_i}{\dot{m}}\frac{d\dot{m}}{dx} \tag{10}$$

All transport equations and detailed chemistry coupling with Arrhenius approach are defined as a set of ordinary differential equations (ODEs). The chemical production term ($\dot{\omega}$) in the reactive part of the equations represents the stiff part of the ODEs set, therefore a stiff ODE solver can operate in different time scales is needed. As also suggested by Zhang et al. [41], the SUNDIALS (Suite of Nonlinear and Differential/Algebraic Equation Solvers) code [44], developed at Lawrence Livermore National Laboratory is chosen for this problem.

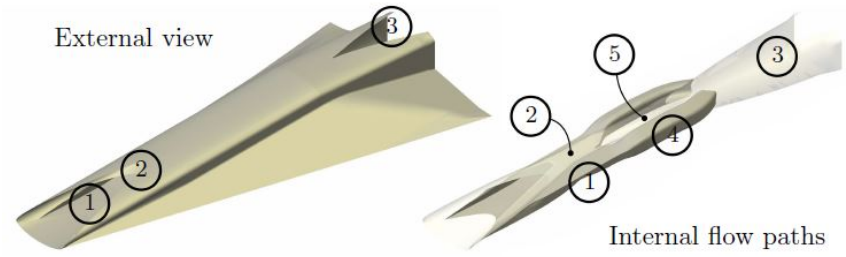

Fig 3. General view of aircraft (left), propulsion path (right) and main components; low speed intake (1), high speed intake (2), common nozzle (3), ATR engine bay (4), DMR engine (5) [49].

2.4. Nozzle design module

The same transport equations in the combustor module are also solved for the inviscid flow in the nozzle. Accordingly, the flow exiting the combustion chamber is perfectly expanded to the ambient conditions through a contoured nozzle [45]. Nevertheless, in accordance to the efficiency and performance specifications exploited for hypersonic cruise [46], Summerfield criteria conditioning the minimum nozzle exit pressure which needs to be higher than 30% of atmospheric pressure is taken into account in the performance examination [31].

3. Results

The proposed low-fidelity design tool is utilized for performing a sample design space analysis over the case study of a novel Mach 5 high-supersonic cruiser for which the employed set of equation and numerical implementation is validated against experimental data (self-reference). The developed concept is considered to be an evolved form of the STRATOLFY MR3 hypersonic civil transportation aircraft [47] with the isolator and combustion chamber characteristics of the propulsive path are preserved, and the main emphasis is made on the influence of intake design variables on the combustion process and the corresponding propulsive performance characterization Fig. 3. The introduced design and analysis module is validated with experimental data obtained by Torrez et al. [25] for ramjet operation at various inflow and fuel feed conditions [48].

3.1. Intake performance

The configurations for the intake design concepts considered in this study are determined by the intensity of the terminating oblique shock and the presence of a secondary internal compression flow upstream of the Busemann contours. In accordance to the value of the startability index[50] and the experimentally proven self-starting characteristics of the MR2.4 intake, the startability index value of S_i ~0.7 is considered as the lower limit for self-startability [51].

$$S_i = \frac{A_s/A_{Isentropic} - 1}{A_{Kantrowitz}/A_{Isentropic} - 1} \tag{11}$$

The issue of unstart arises mainly for the weak shock design configuration due to the considerable demand on isentropic compression to deliver a TPR 95%. Considering the weak deceleration over the terminating shock wave, the Mach number upstream of the shock is also significantly small which requires the contraction ratio to increase for the internal compression flow. This situation violates the physical compressibility limits for allocating the MFRs the intake is being exposed to. The corresponding intakes indicated with *empty* symbols in Fig. 4 (top-1st row) are associated with chocked flow conditions which yields unstart. As $M_{I,E}$ is increased, the isentropic compression requirement on the intake contours is relaxed where the startable intakes are obtained for $M_{I,E}$ >3. In this regard, the ICFA specifications for the weak shock configurations are varied to ensure self-startability by lowering contraction ratio. For smaller $M_{I,E}$ larger wedge angles are required to perform a greater portion of the overall compression over the leading edge shock wave The minimum wedge angle for the ICFA is determined to be 5^o even for the self-starting intakes in order to distinguish the intake performance characteristics from the pure

Busemann contours. Since all intakes designed with a strong shock configuration are associated with a self-starting behavior, the wedge angle for the ICFA is fixed at 5^o.

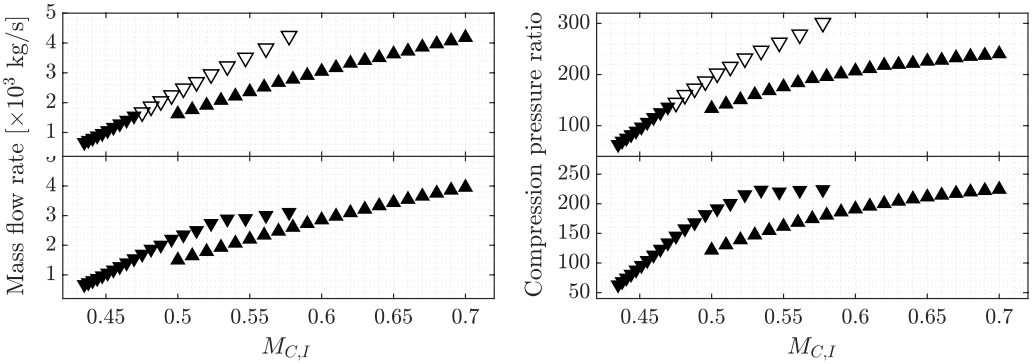

Fig 4. Intake performance parameters of mass flow rate (MFR) (left) and compression pressure ratio (CPR)(right) with weak shock (∇) and strong shock (Δ) configurations of pure Busemann (1^{st} rows) and MBus (2^{nd} rows) concepts. The *filled* and *empty* symbols correspond to the self-starting and unstart intake configurations respectively.

Furthermore, TPR of various intake configurations is dictated by the intensity and the number of shocks since the rest of the compression takes place isentropically. Hence, the corresponding total pressure loss due to the the terminating conical shock can be represented as a function of $M_{I,E}$. Increasing $M_{I,E}$ is associated with an enhanced TPR due to the lower intensity of the terminating oblique shock. Considering the intakes designed with a strong shock configuration, this correlation can be observed directly where the TPR increases with $M_{I,E}$ (Fig. 4, bottom-left 1^{st} row). The additional internal compression flow contour (ICFA) initiated with a conical shock wave located at the leading edge also induces a total pressure loss. Keeping the cruise conditions still, δ_{Ramp} becomes the only parameter to characterize the total pressure variation over the leading edge shock (Fig. 4, bottom-left 2^{nd} row). For both strong and weak shock configurations of fully enclosed Busemann intakes, the resultant TPR appears as a balance of increasing total pressure loss over the conical shock and decreasing total pressure loss over the normal shock at the isolator as $M_{I,E}$ decreases. However, it is observed that the balance favors the influence of the normal shock as its dominance yields lower TPR with increasing $M_{I,E}$. For small $M_{I,E}$, increasing total pressure loss over the intensified leading edge shock and reduced total pressure loss over the weakened normal shock balances each other out. Thus, the TPR levels remain almost constant for the intake exit Mach number range of $2 \leq M_{I,E} \leq 2.4$.

Accordingly, the absence of a normal shock assumption in case of the strong shock configurations, the isentropic relations suggest elevated compression levels with decreasing $M_{I,E}$. Considering the intake exit Mach number range of $0.5 < M_{I,E} < 0.7$, the corresponding isentropic compression ratios are $380 \leq CPR_{S=const} \leq 450$ while the TPR levels are $0.15 \leq \pi \leq 0.6$. Thus, the variation in CPR over the complete range of intake exit Mach number is ~15% of the maximum value ($CPR_{S=const,max}$=450) whilst the variation of TPR is ~75% of the maximum value (π_{max}=0.6). Owing to the dominance of increased total pressure losses, the achieved CPR values are lower (Fig. 4, top-right 1^{st} row). Due to the inverse relationship of $M_{C,I}$ with $M_{I,E}$, the isentropic compression levels increase with increasing $M_{I,E}$ of the weak shock configurations. Nevertheless, as the total pressure losses through the conical and the normal shocks are taken into account, the predominant influence of TPR on the maximum attainable CPR again persists as it was the case for the strong shock configuration (Fig. 4, top-right 2^{nd} row). Moreover, the effect on the temperature ratios is rather straight forward due to the adiabatic nature of the shock waves. For the strong shock configurations, $M_{I,E}$ equals to $M_{C,I}$ so the static temperature ratios over the compression and deceleration process induced by the intake geometries are directly related to $M_{I,E}$. Nonetheless, for weak shock configurations increasing $M_{I,E}$ causes $M_{C,I}$ to get smaller because of the increasing intensity of the isolator normal shock. Therefore, overall deceleration

and the corresponding static temperature increase is inversely related to the supersonic $M_{I,E}$ (Fig. 4, bottom-right).

Finally, investigating the MFR for strong shock configurations, decreasing $M_{I,E}$ reduces the exit static pressure while increasing static temperature $M_{I,E}$. Accordingly, the relations of direct proportionality of $M_{I,E}$ and exit static pressure, and inverse quadratic proportionality of intake exit temperature to MFR are extracted. Thus, there is a directly proportional shift between the MFR values obtained with pure Busemann and MBus concepts that is determined by the TPR ratios (Fig. 4, top-left 1^{st} and 2^{nd} rows). For the weak shock configuration, the represented values are provided as a function of $M_{C,I}$ which is inversely related to the $M_{I,E}$. Thus, with increasing $M_{I,E}$, the significant total pressure losses cause the CPR to decrease and static temperature to increase. Hence, the corresponding MFR decreases with increasing $M_{I,E}$. Furthermore, the dominance of TPR on CPR and the corresponding MFR values, enables the strong shock configurations to have higher MFR through the intake (Fig. 4, top-left 1^{st} row). Finally, the addition of the ICFA upstream of the Busemann contours has a similar effect on the performance of intakes with a weak shock configuration. The increased non-isentropic compression levels while keeping $M_{I,E}$ constant, the ratio of the isentropic compression is reduced. Consequently, due to the dominance of TPR and its corresponding effect on CPR and MFR, the implementation of ICFA allows the accommodation of a larger MFR without rendering the intake contours vulnerable against startability concerns (Fig. 4, top-left 2^{nd} row).

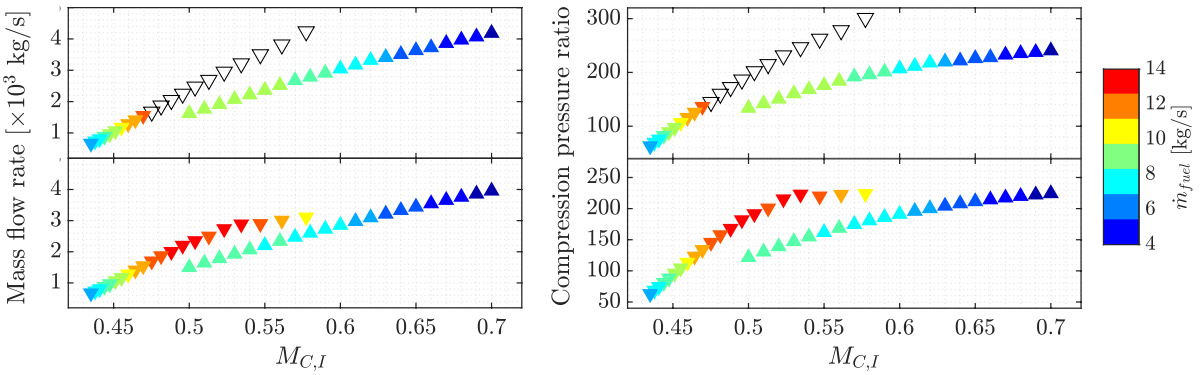

Fig 5. Propulsive performance parameter of fuel consumption ($\dot{m}_f$) in comparison to the intake performance parameters of mass flow rate (MFR)(left) and compression pressure ratio (CPR)(right) with weak shock (∇) and strong shock (Δ) configurations of pure Busemann (1^{st} rows) and MBus (2^{nd} rows) concepts. The *colormapped* and *empty* symbols correspond to the self-starting and unstart intake configurations respectively.

3.2. Propulsive system performance

Fuel consumption ($\dot{m}_f$) is determined by the ramjet module for given pre-combustion flow conditions. For weak shock ICFA inlet designs, it can be said that the acceleration of greater MFR to sonic conditions in the combustor, requires more fuel to be injected. This temperature ratio dominated trend can be seen until the pre-combustion conditions of $M_{C,I}$=0.54. Beyond this point, the change on $M_{C,I}$ does not have any significant influence on MFR and compression ratio for the weak shock ICFA inlet scenarios. This phenomena indicates that ramjet combustion regime highly depends on the initial temperature value of the mixture caused by the highly sensitive nature of combustion kinetics of hydrogen oxidation with air to high initial temperatures. Although initial temperature ratio declines linearly with the increasing $M_{C,I}$, the combustion regime shows nonlinear behavior after Mach 0.54 then there is a remarkable decrease on $\dot{m}_f$. In the regime of low $M_{C,I}$, $\dot{m}_f$ profile of strong shock Busemann intake scenarios follows nearly the same trend of that of ICFA designs. The required $\dot{m}_f$ decreases with $M_{C,I}$ by keeping the trend in the color gradient. This zone can be considered as Mach number dominated region, increase of $M_{C,I}$ reduces the fuel feed needed to achieve sonic condition at the combustor exit despite of dramatically increasing MFR.

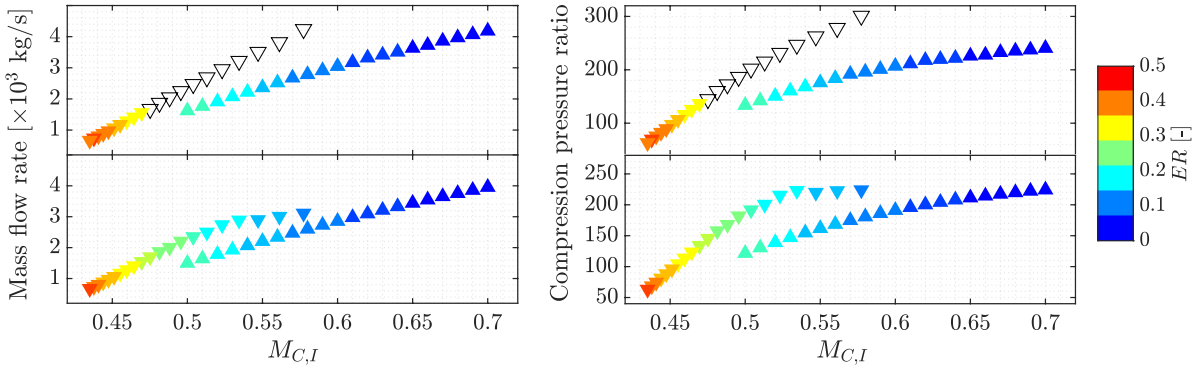

Fig 6. Propulsive performance parameter of equivalence ratio (ER) in comparison to the intake performance parameters of mass flow rate (MFR)(left) and compression pressure ratio (CPR)(right) with weak shock (∇) and strong shock (Δ) configurations of pure Busemann (1^{st} rows) and MBus (2^{nd} rows) concepts. The *colormapped* and *empty* symbols correspond to the self-starting and unstart intake configurations respectively.

As expected, all scenarios are computed in lean burning regime for ramjet operation where the largest ER values are in the highest temperature and lowest CPR zones. For all strong shock scenarios, ER follows similar trends with $\dot{m}_f$ as pointed before. The trend of the $\dot{m}_f$ variation for weak shock ICFA configuration is also observed for ER because of the small increment in MFR and decrease in the $\dot{m}_f$. As seen in Fig. 6 and Fig. 7, the reduction on the ER value with the increase of $M_{C,I}$ for strong shock scenarios has an adverse influence on the uninstalled thrust. The decrease of $\dot{m}_f$ and ER led to insufficient temperature rise along the combustor for increasing MFR. For weak shock inlets, there is an inverse relation between ER and the $\dot{m}_f$ up to $M_{C,I}$=0.55. Towards the limits of the increasing $M_{C,I}$ for the weak shock inlets, the MFR starts to remain constant but ER continues reducing, because $\dot{m}_f$ passes its extremum point and decreases. The flow could reach the sonic limit at the throat with less fuel with the increase of $M_{C,I}$. Considering the uninstalled thrust function, this extremum point was detected as the optimum ER value (ER∼0.2) for the weak shock scenarios (Fig. 7).

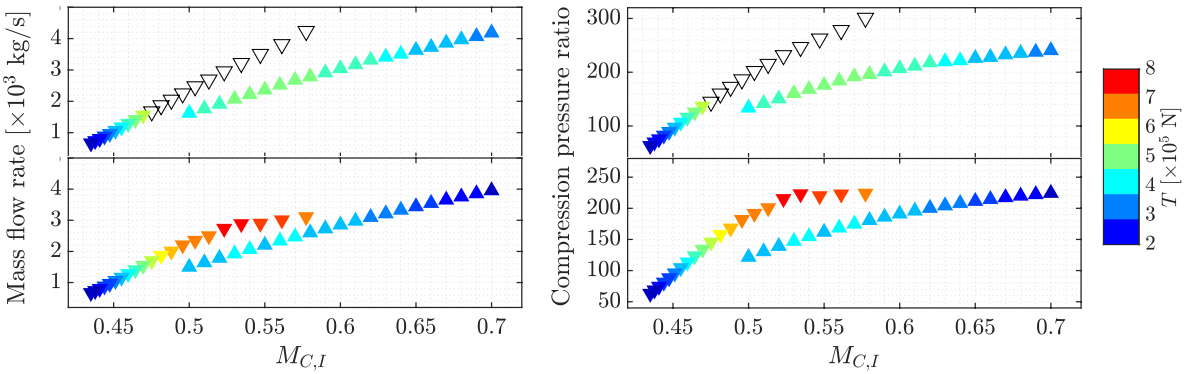

Fig 7. Propulsive performance parameter of uninstalled thrust in comparison to the intake performance parameters of mass flow rate (MFR)(left) and compression pressure ratio (CPR)(right) with weak shock (∇) and strong shock (Δ) configurations of pure Busemann (1^{st} rows) and MBus (2^{nd} rows) concepts. The *colormapped* and *empty* symbols correspond to the self-starting and unstart intake configurations respectively.

Moreover, the increase of $\dot{m}_f$ results in higher chamber exit velocity provides thrust augmentation as observed for $0.5 \leq M_{C,I} \leq 0.6$, Fig. 7 (top-$2^{nd}$ row). Increasing $M_{C,I}$ prevents necessary fuel feed into the chamber because of the lower allowance of expansion to the sonic conditions. Therefore, the thrust is inclined to decrease with the rise of $M_{C,I}$. During the expansion stage in the nozzle, the higher nozzle exit velocity can be obtained in the case of higher TPR. Thus, thrust rises with the TPR until $M_{C,I}$=0.57. After this point, heat release effects (imposed by the $\dot{m}_f$) become more dominant and the thrust value starts to decline for all inlet scenarios. Increasing fuel feed into the combustion chamber provides a greater temperature rise which corresponds to a raised flow velocity at the combustion chamber exit. The counter acting influence of increasing mass flow rate and decreasing fuel feed as $M_{C,I}$ values are increased, results in a range of combustion chamber inlet conditions that provide the greatest thrust values within the range of $0.53 \leq M_{C,I} \leq 0.57$.

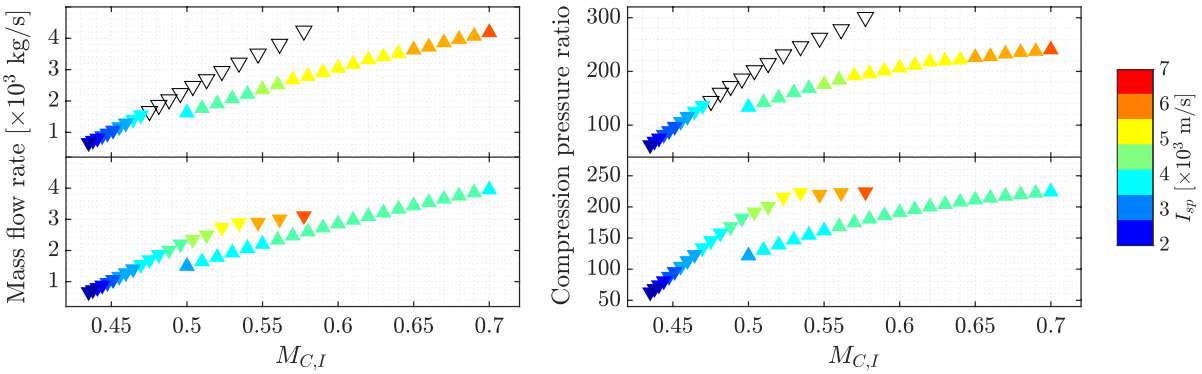

Fig 8. Propulsive performance parameter of specific impulse (I_{sp}) in comparison to the intake performance parameters of mass flow rate (MFR)(left) and compression pressure ratio (CPR)(right) with weak shock (∇) and strong shock (Δ) configurations of pure Busemann (1^{st} rows) and MBus (2^{nd} rows) concepts. The *colormapped* and *empty* symbols correspond to the self-starting and unstart intake configurations respectively.

As seen in Fig. 8, highest and lowest I_{sp} values were obtained where maximum and minimum thrust productions were computed, respectively. Due to the substantial reduction on the $\dot{m}_f$ with the increasing of $M_{C,I}$ for strong shock MBus inlets, I_{sp} reaches the highest values and propulsive efficiency keeps on rising. Moreover, I_{sp} values are found to be higher for the pure Busemann intakes compared to ICFA scenario in the high $M_{C,I}$ regions. This difference is highly caused by the uninstalled thrust since sonic conditions at throat were reached with almost identical fuel consumption levels. Moreover, the MFR significantly influences the $\dot{m}_f$ in some of the $M_{C,I}$ ranges on the performance maps. On the other hand, there is a distinct difference between $\dot{m}_f$ thereby uninstall thrust in middle of investigated Mach number range for strong shock intake scenarios. On the lower end of $M_{C,I}$ range, the uninstalled thrust values were calculated to be quite low due to the low CPR and low MFR. However, $\dot{m}_f$ becomes too close to the intermediary levels of the investigated $M_{C,I}$ range. This caused the ramjet engine to operate with very low I_{sp} in this region.

4. Conclusions

Low fidelity analysis of propulsion systems enable the reduction of complexity involved with the highly three dimensional flow structures and provide a unique opportunity for extensive design space exploration. In this regard, the present study concentrates on 1D modelling of generic high-speed propulsive flow paths based on ramjet engines. The propulsive paths are separated to individual components of intake, isolator, combustor and nozzle where each component is modeled by relevant physical relations. Accordingly, the intake module is based on axisymmetric flow contours provided by internal compression flows of Busemann diffuser and ICFA. Moreover, the 1D steady inviscid flow equations coupled with detailed chemistry approach and JANAF tables, are solved for modeling the flow along the adia-

batic constant-area combustor and diverged nozzle components of the propulsive path.

The intakes designed with the pure Busemann concepts revealed a clear characterization in terms of vulnerablilitz against unstart based on inlet exit Mach numbers ($M_{I,E}$) while the addition of ICFA ensured self-startability. The TPR values are observed to be the dominant factor determining the scales of CPR and MFR obtained at different design points which is covered by varying the design parameter of $M_{I,E}$. Furthermore, two different configurations of weak and shock strong design approaches yielded different trends of TPR. Accordingly, decreasing $M_{I,E}$ values resulted in CPR values following the exact trend of TPR for strong shock configurations while the situation is reversed for weak shock configurations due to the increasing intensity of isolator normal shock. Therefore, increasing $M_{I,E}$ values for strong shock configuration yielded increasing MFR without compromising startability while for the weak shock configuration, decreasing $M_{I,E}$ elevated the demand on isentropic compression which hindered the capability of the intakes to self-start. In terms of propulsive performance, the trend of $\dot{m}_f$ was observed to be inversely related to $M_{C,I}$ for all strong shock intake scenarios. The thrust production followed a similar trend to that of $\dot{m}_f$ but it was also highly influenced by MFR especially at low $M_{C,I}$ values. Greater TPR and MFR with increase of the $M_{C,I}$ were not able to prevent the decrements of thrust because of the remarkable decrease on the $\dot{m}_f$ and ER. The I_{sp} value rises with the increase of $M_{C,I}$ for the weak shock scenarios and the best I_{sp} value of it was obtained at corresponding optimal thrust region. On the other hand, for the strong shock MBus intake scenarios, despite of low rate of the uninstalled thrust, the excessive decrease on $\dot{m}_f$ led to have as efficient operating condition of the ramjet as quantified by means of I_{sp}.

Acknowledgments

This project has received funding from the European Union's Horizon 2020 research and innovation programme under grant agreement No 101006856.

References

[1] Dietrich Kuchemann. *The Aerodynamic Design of Aircraft*. AIAA Education Series. AIAA, 2012. ISBN: 978-1-60086-922-8.

[2] "Earth orbit on-orbit operations in near Earth orbit, a necessary second step". In: *Future Spacecraft Propulsion Systems: Enabling Technologies for Space Exploration*. Berlin, Heidelberg: Springer Berlin Heidelberg, 2006, pp. 203–248. ISBN: 978-3-540-37641-5. DOI: 10.1007/3-540-37641-0_6.

[3] Paul Czysz and Jean Vandenkerckhove. "Transatmospheric Launcher Sizing". In: *Scramjet Propulsion*. Chap. 16, pp. 979–1103. DOI: 10.2514/5.9781600866609.0979.1103.

[4] Takeshi Tsuchiya, Yoichi Takenaka, and Hideyuki Taguchi. "Multidisciplinary Design Optimization for Hypersonic Experimental Vehicle". In: *AIAA Journal* 45.7 (2007), pp. 1655–1662. DOI: 10.2514/1.26668.

[5] Steven Walker et al. "Falcon HTV-3X - A Reusable Hypersonic Test Bed". In: *15th AIAA International Space Planes and Hypersonic Systems and Technologies Conference*. 2008. DOI: 10.2514/6.2008-2544.

[6] Joseph Hank, James Murphy, and Richard Mutzman. "The X-51A Scramjet Engine Flight Demonstration Program". In: Apr. 2008. ISBN: 978-1-60086-985-3. DOI: 10.2514/6.2008-2540.

[7] Sannu Molder et al. *Investigations in the Fluid Dynamics of Scramjet Inlets*. Tech. rep. ADA269275. TORONTO UNIV DOWNSVIEW (ONTARIO) INST FOR AEROSPACE STUDIES, 1992.

[8] Guoping Huang, Fengyuan Zuo, and Wenyou Qiao. "Design method of internal waverider inlet under non-uniform upstream for inlet/forebody integration". In: *Aerospace Science and Technology* 74 (2018), pp. 160–172. ISSN: 1270-9638. DOI: https://doi.org/10.1016/j.ast.2018.01.012.

[9] Lance Jacobsen et al. "Starting and Operation of a Streamline-Traced Busemann Inlet at Mach 4". In: *42nd AIAA/ASME/SAE/ASEE Joint Propulsion Conference & Exhibit*. 2006. DOI: 10.2514/6.2006-4508.

[10] Michael K. Smart and Carl A. Trexler. “Mach 4 Performance of Hypersonic Inlet with Rectangular-to-Elliptical Shape Transition”. In: *Journal of Propulsion and Power* 20.2 (2004), pp. 288–293. DOI: 10.2514/1.1296.

[11] Stuart Laurence et al. “An Experimental Investigation of Steady and Unsteady Combustion Phenomena in the HyShot II Combustor”. In: *17th AIAA International Space Planes and Hypersonic Systems and Technologies Conference*. 2001. DOI: 10.2514/6.2011-2310. eprint: https://arc.aiaa.org/doi/pdf/10.2514/6.2011-2310. URL: https://arc.aiaa.org/doi/abs/10.2514/6.2011-2310.

[12] JM Romeskie S Molder. “Modular hypersonic inlets with conical flow”. In: *AGARD Conference Proceedings*. 1968.

[13] Sannu Mölder. “The Busemann Air Intake for Hypersonic Speeds”. In: *Hypersonic Vehicles*. Ed. by Giuseppe Pezzella and Antonio Viviani. Rijeka: IntechOpen, 2019. Chap. 5. DOI: 10.5772/intechopen.82736.

[14] J. Häberle and A. Gülhan. “Investigation of Two-Dimensional Scramjet Inlet Flowfield at Mach 7”. In: *Journal of Propulsion and Power* 24.3 (2008), pp. 446–459. DOI: 10.2514/1.33545.

[15] Patrick Gruhn and Ali Gülhan. “Experimental Investigation of a Hypersonic Inlet with and Without Sidewall Compression”. In: *Journal of Propulsion and Power* 27.3 (2011), pp. 718–729. DOI: 10.2514/1.50347.

[16] Tue Nguyen et al. “Effects of Sidewall Compression and Relaminarization in a Scramjet Inlet”. In: *Journal of Propulsion and Power* 29.3 (2013), pp. 628–638. DOI: 10.2514/1.B34740.

[17] D. V. Gaitonde et al. “Sidewall Interaction in an Asymmetric Simulated Scramjet Inlet Configuration”. In: *Journal of Propulsion and Power* 17.3 (2001), pp. 579–584. DOI: 10.2514/2.5780.

[18] Faure J. Malo-Molina et al. “Three-Dimensional Analysis of a Supersonic Combustor Coupled to Innovative Inward-Turning Inlets”. In: *AIAA Journal* 48.3 (2010), pp. 572–582. DOI: 10.2514/1.43646.

[19] Sean Candon, Eric Loth, and Michael Rybalko. “Near-On-Design Unsteadiness in a Supersonic Low-Boom Inlet”. In: *Journal of Propulsion and Power* 32.2 (2016), pp. 360–372. DOI: 10.2514/1.B35603.

[20] Fengyuan Zuo, Guoping Huang, and Chen Xia. “Investigation of internal-waverider-inlet flow pattern integrated with variable-geometry for TBCC”. In: *Aerospace Science and Technology* 59 (2016), pp. 69–77. ISSN: 1270-9638. DOI: 10.1016/j.ast.2016.10.009.

[21] F. Lanson and J. L. Stollery. “Some hypersonic intake studies”. In: *The Aeronautical Journal (1968)* 110.1105 (2006), pp. 145–156. DOI: 10.1017/S0001924000001123.

[22] Frederick S. Billig and Ajay P. Kothari. “Streamline Tracing: Technique for Designing Hypersonic Vehicles”. In: *Journal of Propulsion and Power* 16.3 (2000), pp. 465–471. DOI: 10.2514/2.5591.

[23] Jicheng Ma et al. “Control-oriented unsteady one-dimensional model for a hydrocarbon regeneratively-cooled scramjet engine”. In: *Aerospace Science and Technology* 85 (2019), pp. 158–170. DOI: 10.1016/j.ast.2018.12.012.

[24] Lu Tian et al. “Quasi-one-dimensional multimodes analysis for dual-mode scramjet”. In: *Journal of Propulsion and Power* 30.6 (2014), pp. 1559–1567. DOI: 10.2514/1.B35177.

[25] Sean M. Torrez et al. “Reduced-Order Modeling of Turbulent Reacting Flows with Application to Ramjets and Scramjets”. In: *Journal of Propulsion and Power* 27.2 (2011), pp. 371–382. DOI: 10.2514/1.50272.

[26] Cristian H Birzer and Con J Doolan. “Quasi-one-dimensional model of hydrogen-fueled scramjet combustors”. In: *Journal of propulsion and power* 25.6 (2009), pp. 1220–1225. DOI: 10.2514/1.43716.

[27] M. G. Owens et al. “Thermal Choking Analyses in a Supersonic Combustor”. In: *Journal of Propulsion and Power* 17.3 (2001), pp. 611–616. DOI: 10.2514/2.5785.

[28] Sean O’Byrne et al. “Analysis of transient thermal choking processes in a model scramjet engine”. In: *36th AIAA Aerospace Sciences Meeting and Exhibit*. 2000, p. 965. DOI: 10.2514/2.5645.

[29] Abraham Cohen-Zur and Benveniste Natan. “Experimental investigation of a supersonic combustion solid fuel ramjet”. In: *Journal of Propulsion and Power* 14.6 (1998), pp. 880–889. DOI: 10.2514/2.5379.

[30] Sean M Torrez, Derek J Dalle, and James F Driscoll. “New method for computing performance of choked reacting flows and ram-to-scram transition”. In: *Journal of Propulsion and Power* 29.2 (2013), pp. 433–445. DOI: 10.2514/1.B34496.
[31] V Fernández-Villace, G Paniagua, and Johan Steelant. “Installed performance evaluation of an air turbo-rocket expander engine”. In: *Aerospace science and technology* 35 (2014), pp. 63–79. DOI: 10.1016/j.ast.2014.03.005.
[32] Sin-I. Cheng. “Hypersonic propulsion”. In: *Progress in Energy and Combustion Science* 15.3 (1989), pp. 183–202. ISSN: 0360-1285. DOI: https://doi.org/10.1016/0360-1285(89)90008-7. URL: https://www.sciencedirect.com/science/article/pii/0360128589900087.
[33] M. K. Smart. “Design of Three-Dimensional Hypersonic Inlets with Rectangular-to-Elliptical Shape Transition”. In: *Journal of Propulsion and Power* 15.3 (1999), pp. 408–416. DOI: 10.2514/2.5459.
[34] John J Mahoney. *Inlets for supersonic missiles*. Amer Inst of Aeronautics &, 1990. ISBN: 978-0-930403-79-9.
[35] John Seddon and E Laurie Goldsmith. *Intake aerodynamics*. Vol. 2. Blackwell science Oxford, 1999. ISBN: 9781563473616.
[36] Sannu Molder. “Internal, axisymmetric, conical flow.” In: *AIAA Journal* 5.7 (1967), pp. 1252–1255. DOI: 10.2514/3.4179.
[37] R. Courant and K.O. Friedrichs. *Supersonic Flow and Shock Waves*. Applied Mathematical Sciences. Springer New York, 1999. ISBN: 9780387902326.
[38] P.A. Thompson. *Compressible-fluid Dynamics*. Advanced engineering series. McGraw-Hill, 1971. ISBN: 9780070644052.
[39] J.C. Butcher. “A history of Runge-Kutta methods”. In: *Applied Numerical Mathematics* 20.3 (1996), pp. 247–260. ISSN: 0168-9274. DOI: 10.1016/0168-9274(95)00108-5.
[40] Pedro M Goncalves, Ali C Ispir, and Bayindir H Saracoglu. “Development and optimization of a hypersonic civil aircraft propulsion plant with regenerator system”. In: *AIAA Propulsion and Energy 2019 Forum*. 2019, p. 4421. DOI: 10.2514/6.2019-4421.
[41] Duo Zhang et al. “Quasi-one-dimensional model of scramjet combustor coupled with regenerative cooling”. In: *Journal of Propulsion and Power* 32.3 (2016), pp. 687–697. DOI: 10.2514/1.B35887.
[42] Casimir J Jachimowski. “An analytical study of the hydrogen-air reaction mechanism with application to scramjet combustion”. In: (1988).
[43] Bonnie J McBride. *Coefficients for calculating thermodynamic and transport properties of individual species*. Vol. 4513. NASA Langley Research Center, 1993.
[44] Alan C Hindmarsh et al. “SUNDIALS: Suite of nonlinear and differential/algebraic equation solvers”. In: *ACM Transactions on Mathematical Software (TOMS)* 31.3 (2005), pp. 363–396. DOI: 10.1145/1089014.1089020.
[45] Ali C Ispir, Pedro M Goncalves, and Bayindir H Saracoglu. “Thermodynamic efficiency analysis and investigation of exergetic effectiveness of STRATOFLY aircraft propulsion plant”. In: *AIAA Scitech 2020 Forum*. 2020, p. 1108. DOI: 10.2514/6.2020-1108.
[46] Johan Steelant et al. “Achievements obtained for sustained hypersonic flight within the LAPCAT-II project”. In: *20th AIAA international space planes and hypersonic systems and technologies conference*. 2015, p. 3677. DOI: 10.2514/6.2015-3677.
[47] Roberta Fusaro and Nicole Viola. “Design and integration of a cryogenic propellant subsystem for the hypersonic STRATOFLY MR3 Vehicle”. In: *AIAA Scitech 2020 Forum*. 2020, p. 1106. DOI: 10.2514/6.2020-1106.
[48] Bora O. Cakir, Ali Can Ispir, and Bayindir H. Saracoglu. “Reduced order design and investigation of intakes for high speed propulsion systems”. In: *Acta Astronautica* 199 (2022), pp. 259–276. ISSN: 0094-5765. DOI: https://doi.org/10.1016/j.actaastro.2022.07.037.
[49] Víctor Fernández Villacé. “Simulation, Design and Analysis of Air-Breathing Combined-Cycle Engines for High Speed Propulsion”. PhD thesis. Escula Técnica Superior De Ingenieros Aeronáuticos, 2013.
[50] Niloofar Moradian et al. “Startability analysis of Busemann intakes with overboard spillage”. In: June 2014. ISBN: 978-1-62410-284-4. DOI: 10.2514/6.2014-3227.
[51] Johan Steelant and Tobias Langener. “The LAPCAT-MR2 hypersonic cruiser concept”. In: 2014.